Passive Earth Pressure on a Vertical Retaining Wall with Horizontal Cohesionless Backfill

G.S. Kame, D.M. Dewaikar, D. Choudhury

Abstract. A method based on the application of Kötter's equation is proposed for the complete analysis of passive earth pressure on a vertical wall retaining horizontal cohesionless backfill. The unique failure surface consisting of log spiral and its tangent is identified on the basis of force equilibrium conditions. One distinguishing feature of the proposed method is its ability to compute the point of application of passive thrust using moment equilibrium. Another distinguishing feature is the prediction of distribution of soil reaction on the failure surface. The results show a close agreement with some of the available solutions.

Keywords: Kötter's equation, passive earth pressure coefficient, cohesionless soil, log spiral, point of application, horizontal backfill.

1. Introduction

Earth retaining structures such as sheet piles, retaining walls, wing walls, abutments and bulkheads are very common in engineering practices. While retaining earth, these structures are subjected to lateral earth pressures. Anchors of the bulkhead and vertical plate anchors are some of the structures which are located very near to ground level and subjected to passive earth pressure of the retained cohesionless soil.

Coulomb (1776) and Rankine (1857) proposed methods for the estimation of earth pressure on retaining walls based on the assumption of a plane failure surface. For the limit equilibrium analysis of passive thrust on retaining wall, Terzaghi (1943) proposed a failure mechanism, in which, the failure surface consisted of a log spiral originating from the wall base, followed by a tangent, that met the ground surface at an angle corresponding to Rankine's passive state. Several other research workers have adopted this failure mechanism.

Caquot & Kerisel (1948) and Kerisel & Absi (1990) proposed a log spiral mechanism and presented their results in the form of charts. Janbu (1957), Sheilds & Tolunay (1973), Basudhar & Madhav (1980), and Kumar & Subba Rao (1997) used method of slices for computing passive pressure coefficients in respect of a cohesionless soil by considering soil mass in a state of limit equilibrium.

Morgenstern & Eisenstein (1970) compared the values of passive earth pressure coefficient K_p calculated with the theories proposed by Caquot & Kerisel (1948), Brinch-Hansen (1953), Janbu (1957) and Sokolovski (1965). They concluded that with the assumption of a plane failure surface, Coulomb's (1776) theory overestimated the passive resistance.

Lancellotta (2002) provided an analytical solution for the passive earth pressure coefficients, based on the lower bound theorem of plasticity. Soubra & Macuh (2002) used an approach based on rotational log-spiral failure mechanism with the upper-bound theorem of limit analysis for the analysis of passive earth pressures.

In the recent past, Shiau *et al.* (2008) have reported the values of passive earth pressure coefficient using upper and lower bound theorems of limit analysis coupled with finite element formulation and nonlinear programming techniques.

From the review of literature, it is observed that, Kötter's (1903) equation has been employed (Balla, 1961 and Matsuo, 1967) to evaluate soil shearing resistance on a curved failure surface. Dewaikar & Mohapatro (2003) used Kötter's (1903) equation for computation of bearing capacity factor, N_γ for shallow foundations.

In the proposed investigations, a method is developed using Kötter's (1903) equation for the computation of passive thrust and its point of application for a vertical wall retaining horizontal cohesionless backfill, using the failure mechanism suggested by Terzaghi (1943). The distribution of soil reaction on the failure surface is also evaluated.

2. Proposed Method

The proposed method is an attempt to analyse the capacity of vertical plate anchors which are shallow or deep laid in cohesionless soil. The basic case refers to the situation where the plate anchor is flushing with the ground surface and involves estimation of the passive thrust. The same is analysed here.

Figure 1 shows a vertical retaining wall DE, with a horizontal cohesionless backfill. The failure surface con-

G.S.Kame, Research Scholar, Department of Civil Engineering, Indian Institute of Technology, 400076 Bombay, Powai, Mumbai, India. e-mail: gskame@iitb.ac.in.
D.M. Dewaikar, PhD, Professor, Department of Civil Engineering, Indian Institute of Technology, 400076 Bombay, Powai, Mumbai, India. e-mail: dmde@civil.iitb.ac.in.
D. Choudhury, PhD, Associate Professor, Department of Civil Engineering, Indian Institute of Technology, 400076 Bombay, Powai, Mumbai, India. e-mail: dc@civil.iitb.ac.in.
Submitted on October 1, 2010; Final Acceptance on February 14, 2011; Discussion open until April 30, 2012.

sists of log spiral EA, that originates from wall base, with tangent, AB meeting the ground surface at an angle, (45° - ϕ/2), where, ϕ is the angle of soil internal friction. At A, there is a conjugate failure plane AD, passing through the wall top. Thus, as seen from the figure, ABD is a passive Rankine zone and pole of the log spiral lies on the line AD or its extension and this is also shown in Figs. 2(a) and 2(b).

From Fig. 1, the following information is generated:

H = height of the retaining wall,

α = inclination of the tangent to the log spiral at point G with the horizontal,

θ = spiral angle measured from the starting radius,

r_0 = starting radius of the log spiral at the wall base (at $\theta = 0$),

r = radius of log spiral at point G corresponding to the spiral angle θ,

θ_m = maximum spiral angle,

r_1 = radius of the maximum spiral angle at $\theta = \theta_m$,

θ_v = angle between vertical face of the wall and the starting radius r_0.

Figures 2(a) and 2(b) show the location of pole of the log spiral when it is located above and below the wall top respectively. From Fig. 2(b), the following additional information is generated.

θ_A = angle between vertical face of the wall and line OD when pole is located below the wall top.

θ_S = angle between the radius r_0 and line OD when pole is located below the* wall top.

From Figs. 3(a) and 3(b), which show free body diagrams of failure wedge EABCD, the following information is generated.

P_{pH}, P_{pV} = horizontal and vertical components of resultant passive thrust, P_p,

R_H, R_V = horizontal and vertical components of resultant soil reaction acting on the curved part of the failure surface,

H_1 = active thrust exerted by the backfill on the Rankine wall AC,

W_{ACD} = weight of soil in the failure wedge, forming a part of the Rankine zone,

W_{ADE} = weight of soil in the zone, EAD of the failure wedge, EABCD.

In Fig 3(a), line AC represents the Rankine wall and force, H_1 as described above, is the force exerted on this wall by the backfill it retains. With this consideration and also considering that pole of the log spiral lies above the wall top on line AD, the dispositions of various forces are shown in the same figure.

In Fig. 3(b), which refers to location of pole, O below the wall top, in addition to forces mentioned earlier, forces, W_{ODE} and W_{OEA} together represent the weight of portion EAD of the failure wedge, EACD, as shown in the same figure.

2.1. Geometry of failure surface

This is dependent upon the location of pole of the log spiral.

2.1.1. Pole above wall top

Referring to Fig. 2(a) and considering triangle, ODE,

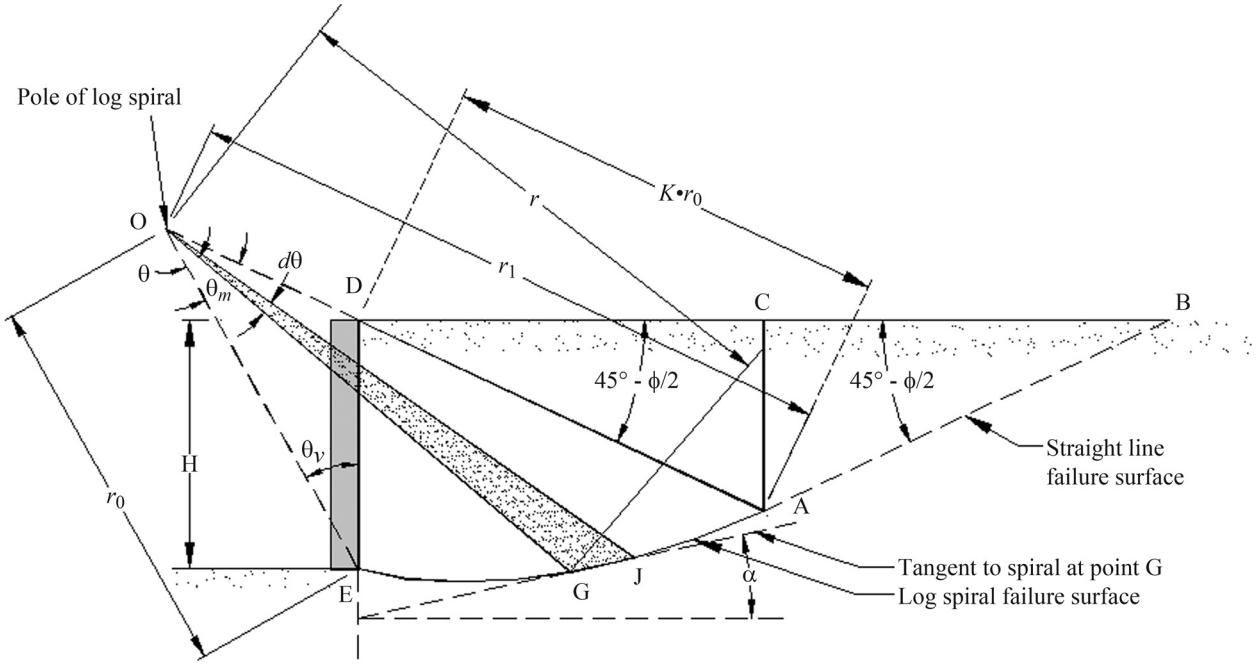

Figure 1 - Retaining wall with a horizontal cohesionless backfill - failure mechanism.

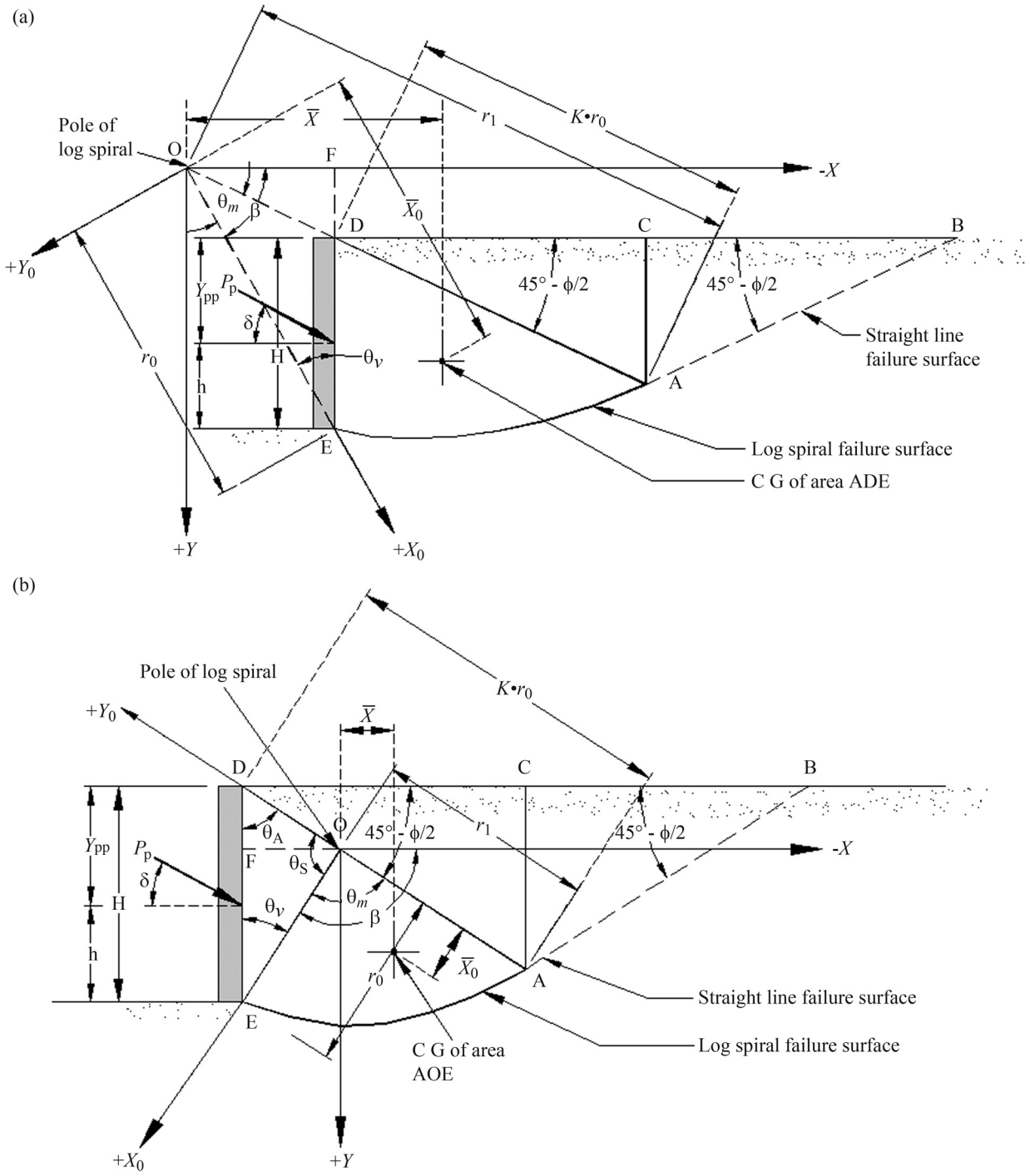

Figure 2 - (a) Failure surface adopted in the proposed analysis with pole located above the wall top. (b) Failure surface adopted in the proposed analysis with pole located below the wall top.

$$\frac{OD}{\sin\theta_v} = \frac{OE}{\sin\left\{135 - \frac{\phi}{2}\right\}} = \frac{DE}{\sin\theta_m} = \frac{H}{\sin\theta_m} \qquad (1)$$

In which, angles, θ_m and θ_v are as shown in the same figure.

From the above expression,

$$OD = \frac{H \sin\theta_v}{\sin\theta_m}$$

The initial radius, OE = r_0 of the log spiral is given as

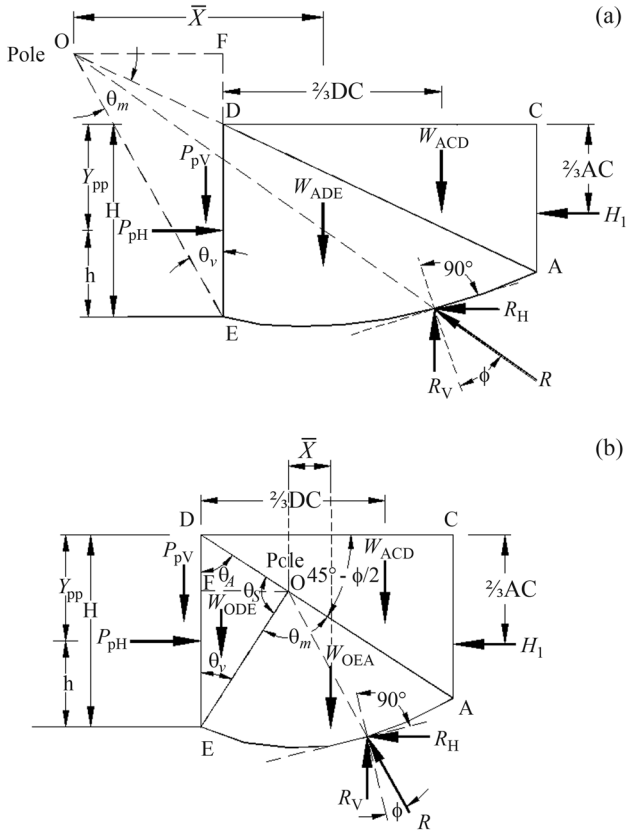

Figure 3 - (a) Free body diagram of failure wedge EACD with pole above the wall top. (b) Free body diagram of failure wedge EACD with pole below the wall top.

$$OE = r_0 = \frac{H \sin\left\{135 - \frac{\phi}{2}\right\}}{\sin\theta_m}$$

Also, from the equation of the log spiral,

$$OA = r_0 \cdot e^{\theta_m \tan\phi}$$

and

$$AD = OA - OD$$

2.1.2. Pole below wall top

Referring to Fig. 2(b) and considering triangle ODE,

$$\frac{OD}{\sin\theta_v} = \frac{OE}{\sin\theta_A} = \frac{DE}{\sin\theta_S} = \frac{H}{\sin\theta_S} \quad (2)$$

From which, the initial radius, OE = r_0, of the log spiral is given as

$$OE = r_0 = \frac{H \sin\theta_A}{\sin\theta_S}$$

and

$$OD = \frac{H \sin\theta_v}{\sin\theta_S}$$

Also, from the equation of the log spiral,

$$OA = r_0 \cdot e^{\theta_m \tan\phi}$$

and

$$AD = OA + OD$$

2.2. Computation of soil reaction on the failure surface

Kötter's (1903) equation basically refers to the distribution of reactive pressure on the failure surface, in a cohesionless soil medium and for the passive state of equilibrium (Fig. 4), it is as given below:

$$\frac{dp}{ds} + 2p\tan\phi\frac{d\alpha}{ds} = \gamma\sin(\alpha+\phi) \quad (3)$$

in which dp = differential reactive pressure on the failure surface, ds = differential length of arc of failure surface, ϕ = angle of soil internal friction, $d\alpha$ = differential angle, γ = unit weight of soil and, and α = inclination of the tangent at the point of interest with the horizontal.

The failure surface as shown in Fig.1 has two parts; EA, which is curved and AB, which is a straight line. Kötter's (1903) equation is used to obtain the distribution of reactive pressure on both these parts.

2.2.1. Computation of soil reaction on plane failure surface AB

For a plane failure surface, $d\alpha/ds = 0$ and Eq. (3) takes the following form:

$$\frac{dp}{ds} = \gamma\sin(\alpha+\phi) \quad (4)$$

Integration of the above equation gives

$$p = \gamma\sin(\alpha+\phi) + C_1 \quad (5)$$

Equation (5) gives distribution of reaction on the plane failure surface, AB. The distance, s is measured from

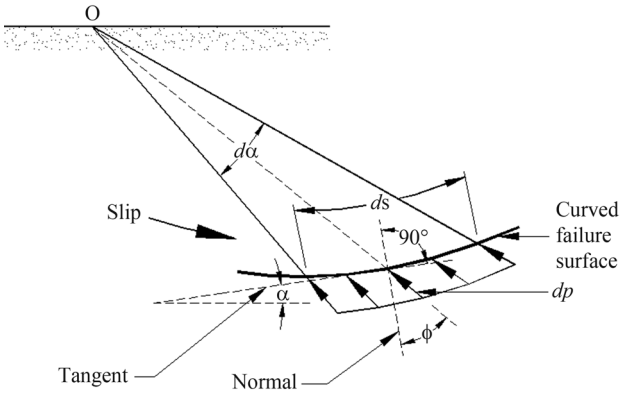

Figure 4 - Reactive pressure distribution on the failure surface for passive case.

point B (Fig. 1). The integration constant, C_1 is evaluated from the boundary condition that, pressure, p is zero at point B, which corresponds to $s = 0$. With this condition, C_1 is zero and Eq. (5) becomes

$$p = \gamma \sin(\alpha + \phi) s \tag{6}$$

In the above equation, $\alpha = 45 - \phi/2$ and with this substitution one obtains

$$p = \gamma \sin(45 + \phi/2) s \tag{7}$$

At point A (Fig. 1), p is given as

$$p = \gamma \sin(\alpha + \phi) \mathrm{AB} \tag{8}$$

The distance, AB depends upon the location of pole of log spiral, *i.e.*, whether it lies below or above the wall top.

2.2.2. Computation of vertical and horizontal components of reaction on curved failure surface EA

Multiplying Eq. (3) throughout by $ds/d\alpha$ and rearranging, the following equation is obtained:

$$\frac{dp}{d\alpha} + 2p \tan\phi = \gamma \sin t \frac{ds}{d\alpha} \tag{9}$$

In which

$$t = (\alpha + \phi), \text{ with } d\alpha = dt \tag{10}$$

From the geometry of log spiral,

$$\frac{ds}{d\theta} = r \sec\phi \tag{11}$$

From Fig. 1, the angle, α is evaluated in terms of log spiral angle, θ as given below:

$$\alpha = \theta - (90 - \theta_V)$$

with $(90 - \theta_V) = \theta_L$, α is written as

$$\alpha = \theta - \theta_L \text{ and } d\alpha = d\theta \tag{12}$$

From Eqs. (10) and (12), θ is obtained as

$$\theta = t + \theta_L - \phi \tag{13}$$

After making necessary substitutions in Eq. (9) the following equation is obtained.

$$\frac{dp}{dt} + 2p \tan\phi = \gamma \sin t \frac{ds}{d\theta} \tag{14}$$

Using Eq. (11), the above equation is written as

$$\frac{dp}{dt} + 2p \tan\phi = \gamma \sin t r \sec\phi \tag{15}$$

With $r = r_0 e^{\theta \tan\phi}$ the above equation is transformed to

$$\frac{dp}{dt} + 2p \tan\phi = \gamma \sin t r_0 \, e^{\theta \tan\phi} \sec\phi \tag{16}$$

Substitution of the value of θ from Eq. (13), in Eq. (16) gives the following equation.

$$\frac{dp}{dt} + 2p \tan\phi = \gamma \sec\phi r_0 \, e^{(t + \theta_L - \phi)\tan\phi} \sin t \tag{17}$$

The solution of above differential equation is obtained as

$$p = \gamma \cdot r_0 \sec\phi e^{(3\theta_L - 2\theta - 3\phi)\tan\phi} [p_1 + C_2] \tag{18}$$

where

$$p_1 = \left[\frac{e^{(3\tan\phi)(\theta - \theta_L + \phi)} [3\tan\phi(\theta - \theta_L + \phi) - \cos(\theta - \theta_L + \phi)]}{(1 + 9\tan^2\phi)} \right] \tag{19}$$

C_2 is the constant of integration and it is obtained from the boundary condition that, at Point A (Fig. 1) with , reaction is as calculated from Eq. (8).

$$C_2 = \frac{e^{(3\tan\phi)(\theta_m - \theta_L + \phi)}}{(1 + 9\tan^2\phi)} \left\{ K \cos\phi \sin\left(\frac{\pi}{4} + \frac{\phi}{2}\right)(1 + 9\tan^2\phi) - [3\tan\phi \sin(\theta_m - \theta_L + \phi) - \cos(\theta_m - \theta_L + \phi)] \right\} \tag{20}$$

With the above value of C_2, pressure distribution on the curved surface is given as

$$p = \left[\gamma r_0 K \sin\left(\frac{\pi}{4} + \frac{\phi}{2}\right) e^{\tan\phi(3\theta_m - 2\theta)} + \frac{\gamma r_0 \sec\phi e^{\theta\tan\phi}}{(1 + 9\tan^2\phi)} (3\tan\phi \sin(\theta - \theta_L + \phi) - \cos(\theta - \theta_L + \phi)) - \frac{\gamma r_0 \sec\phi e^{\tan\phi(3\theta_m - 2\theta)}}{(1 + 9\tan^2\phi)} \times (3\tan\phi \sin(\theta_m - \theta_L + \phi) - \cos(\theta_m - \theta_L + \phi)) \right] \tag{21}$$

where K is the parameter indicating location of the pole of the log spiral along line AO in terms of radius r_0 measured from point D (Fig. 1).

The expression for K is given as

$$K = \left[1 - \frac{\mathrm{OD}/r_0}{e^{\theta_m \tan\phi}} \right], \text{ for pole above wall top (Fig.2 (a))}$$

and

$$K = \left[1 + \frac{\mathrm{OD}/r_0}{e^{\theta_m \tan\phi}} \right], \text{ for pole below wall top (Fig.2 (b))}$$

2.3. Components of resultant soil reaction on the failure surface

The resultant soil reaction, R on the failure surface is given as

$$R = \int p \cdot ds \tag{22}$$

The vertical component, R_V (Fig. 3) of resultant soil reaction is obtained as

$$R_V = \int_0^{\theta_m} p\cos(\theta - \theta_L + \phi)ds \tag{23}$$

Using Eq. (11),

$$R_V = \int_0^{\theta_m} pr_0 e^{\theta\tan\phi}\cos(\theta - \theta_L + \phi)\sec\phi d\theta \tag{24}$$

After substituting the value of p from Eq. (21), R_V is obtained in the following form after carrying out integrations.

$$R_V = R_{V1} + R_{V2} + R_{V3} \tag{25a}$$

where

$$R_{V1} = \gamma r_0^2 K\left[\left\{e^{3\tan\phi\theta_m}\sin\left(\frac{\pi}{4}+\frac{\phi}{2}\right)\right\}\times \left\{e^{-\tan\phi_m}\sin\left(\frac{\pi}{4}-\frac{\phi}{2}\right) - \sin\sin\left(\frac{\pi}{4}-\theta_m-\frac{\phi}{2}\right)\right\}\right] \tag{25b}$$

$$R_{V2} = \frac{\gamma r_0^2\sec^2\phi}{4(1+9\tan^2\phi)}\left[\left\{\frac{3\tan\phi}{\sec\phi}\left[e^{2\tan\phi\theta_m}\sin 2\phi + \sin 2(\theta_m-\phi)\right]\right\} - \left\{\frac{1}{\tan\phi}\left[e^{2\phi_m\tan\phi}-1\right] + \frac{1}{\sec\phi}\left[e^{2\theta_m\tan\phi}\cos 2\phi - \cos\left(2\phi - 2^{\theta_m}\right)\right]\right\}\right] \tag{25c}$$

and

$$R_{V3} = -\frac{\gamma r_0^2\sec^2\phi e^{3\tan\phi\theta_m}}{(1+9\tan^2\phi)}\left[\left\{e^{-\theta_m\tan\phi}\sin\left(\frac{\pi}{4}-\frac{\phi}{2}\right) - \sin\left(\frac{\pi}{4}-\theta_m-\frac{\phi}{2}\right)\right\}\times\left\{3\tan\phi\sin\left(\frac{\pi}{4}+\frac{\phi}{2}\right) - \cos\left(\frac{\pi}{4}+\frac{\phi}{2}\right)\right\}\right] \tag{25d}$$

Similarly, the horizontal component, R_H (Fig. 3) of soil reaction is given as

$$R_H = \int_0^{\theta_m} pr_0 e^{\theta\tan\phi}\sin(\theta - \theta_L + \phi)\sec\phi d\theta \tag{26}$$

After substituting the value of p from Eq. (21), R_H is obtained in the following form after carrying out integrations.

$$R_H = R_{H1} + R_{H2} + R_{H3} \tag{27a}$$

where

$$R_{H1} = \gamma r_0^2 K\left[\left\{e^{3\tan\phi\theta_m}\sin\left(\frac{\pi}{4}+\frac{\phi}{2}\right)\right\}\times \left\{\cos\left(\frac{\pi}{4}-\theta_m-\frac{\phi}{2}\right)\right\} - e^{-\tan\phi\theta_m}\cos\left(\frac{\pi}{4}-\frac{\phi}{2}\right)\right] \tag{27b}$$

$$R_{H2} = \frac{\gamma r_0^2\sec^2\phi}{4(1+9\tan^2\phi)}\left\{3\tan\phi\left[\frac{1}{\tan\phi}(e^{2\theta_m\tan\phi}-1) - \frac{1}{\sec\phi}[e^{2\theta_m\tan\phi}\cos(2\phi) - \cos(2\phi - 2\theta_m)]\right] - \frac{1}{\sec\phi}\left(e^{2\tan\phi_m}\sin(2\phi) + \sin(2\theta_m - 2\phi)\right)\right\} \tag{27c}$$

and

$$R_{H3} = \frac{\gamma r_0^2\sec^2\phi e^{3\tan\phi\theta_m}}{(1+9\tan^2\phi)}\left\{\left[3\tan\phi\sin\left(\frac{\pi}{4}+\frac{\phi}{2}\right) - \cos\left(\frac{\pi}{4}+\frac{\phi}{2}\right)\right]\times\left[\cos\left(\frac{\pi}{4}-\theta_m-\frac{\phi}{2}\right) - e^{-\tan\phi\theta_m}\cos\left(\frac{\pi}{4}-\frac{\phi}{2}\right)\right]\right\} \tag{27d}$$

2.4. Magnitude of passive thrust

In Fig. 3, the active Rankine thrust H_1 acts at a distance 2/3 AC from point, C. Static equilibrium of wedge, EACD is then considered.

Vertical force equilibrium condition gives

$$P_{pV} = P_p\sin\delta = R_v - W_{ACD} - W_{ADE} \tag{28}$$

From which, P_p is obtained as

$$P_p = \frac{R_v - W_{ACD} - W_{ADE}}{\sin\delta} \tag{29}$$

Horizontal force equilibrium condition gives

$$P_{pH} = P_p\cos\delta = R_H + H_1 \tag{30}$$

From which, P_p is obtained as

$$P_p = \frac{R_H + H_1}{\cos\delta} \tag{31}$$

It may be noted that, both Eqs. (29) and (31) give the magnitude of unknown thrust, P_p. These two equations will yield the same and unique value of P_p only when the equilibrium conditions correspond to those at failure, which are uniquely defined by a characteristic value of θ_V and this value can be determined by trial and error procedure.

2.5. Trial and error procedure

In this procedure, first a trial value of θ_V is assumed and corresponding weight of trial failure wedge, EACD (Fig. 3) is computed. Using Eqs. (25) and (27), magnitudes of vertical and horizontal components of soil reaction (R_V

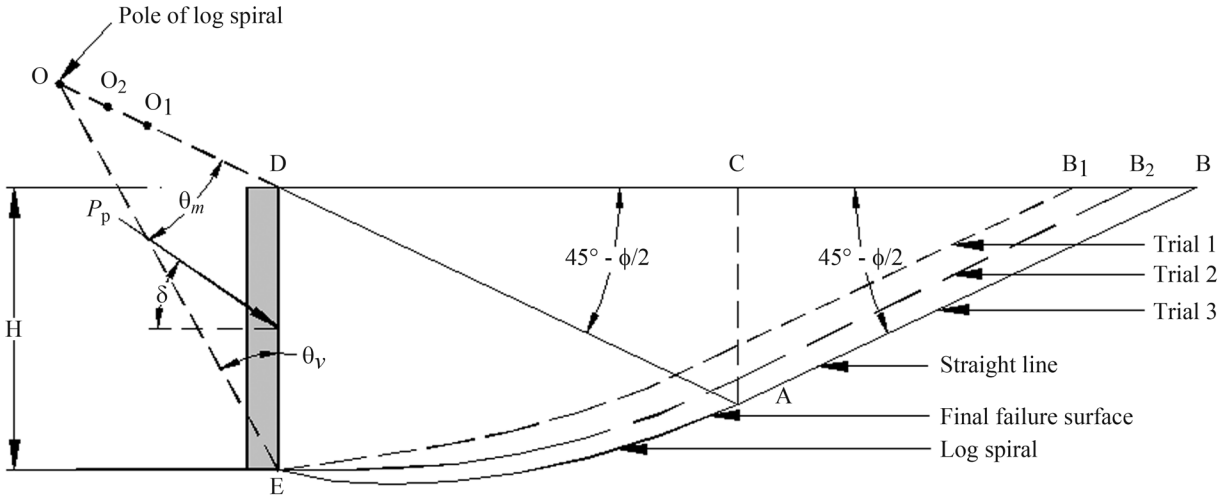

Figure 5 - Trial procedure for locating pole of the log spiral.

and R_H) are computed and from Eqs. (29) and (31), values of P_p are determined. If the trial value of θ_v is equal to its characteristic value corresponding to the failure condition, the two computed values of P_p will be the same; otherwise, they will be different.

For various trial values of θ_v, computations are carried out till the convergence is reached to a specified (third) decimal accuracy.

Thus, in this method of analysis, the unique failure surface (Fig. 5) is identified by locating the pole of log spiral in such a manner that, force equilibrium condition of failure wedge, EACD is satisfied. This approach is different from other analyses in which, P_p is obtained from the consideration of its minimum value.

The passive earth pressure coefficient, K_p is expressed as

$$K_p = \frac{2P_p}{\gamma H^2} \tag{32}$$

Values of passive earth pressure coefficient, K_p are obtained for different values of angles of soil internal friction, ϕ and wall friction, δ.

2.6. Centroid of log spiral

These calculation are performed with reference to Fig. 2(a) (for pole of the log spiral above the wall top) and Fig. 2(b) (for pole of the log spiral below the wall top) respectively. Axis, X_0 is taken along the line that joins pole, O of the log spiral to the wall base. Axis, Y_0 is perpendicular to the axis, X_0 and passes through pole of the log spiral. With respect to these axes, coordinates of the centroid of area inscribed in the log spiral are given as,

$$\bar{X}_0 = \frac{-4r_0}{3}\frac{\tan\phi}{(1+9\tan^2\phi)}\times \left[\frac{e^{3\tan\phi\theta_m}(\sin\theta_m + 3\tan\phi\cos\theta_m) - 3\tan\phi}{e^{2\tan\phi\theta_m} - 1}\right] \tag{33}$$

$$\bar{Y}_0 = \frac{-4r_0}{3}\frac{\tan\phi}{(1+9\tan^2\phi)}\times \left[\frac{e^{3\tan\phi\theta_m}(3\tan\phi\sin\theta_m - \cos\theta_m) - 1}{e^{2\tan\phi\theta_m} - 1}\right] \tag{34}$$

where, r_0 is radius of arc of log spiral at the base of retaining wall, *i.e.* at $\theta = 0°$.

Axes, X and Y are another set of coordinate axes. Axis, X passes through the pole of log spiral and is horizontal. Axis, Y is perpendicular to X axis and passes through the pole, O. With reference to these axes, the coordinates, of centroid of log spiral are given as

$$\bar{X} = \bar{Y}_0 \sin\beta + \bar{X}_0 \cos\beta \tag{35}$$

$$\bar{Y} = \bar{Y}_0 \cos\beta - \bar{X}_0 \sin\beta \tag{36}$$

where, β is the angle made by the axis, X_0 with horizontal.

2.7. Point of application of passive thrust

Moment equilibrium condition is now used to compute the point of application of passive thrust by considering moments of forces and reactions about the pole of the log spiral.

2.7.1. Pole above wall top

Referring to Fig. 3(a), the following moment equilibrium equation is obtained.

$$P_{pH}(Y_{pp} + FD) = \left[\left(W_{ACD}\cdot(OF + \tfrac{2}{3}\cdot DC) + W_{ADE}\cdot\bar{X}\right) + H_1(\tfrac{2}{3}\cdot AC + FD) + P_{pV}\cdot OF\right] \tag{37}$$

In which, the terms on the right hand side of the above expression represent moment of weight of soil in the failure wedge, EACD, moment of the force H_1 and moment due to vertical component of the resultant passive thrust, P_{pV} about the pole, O. The term on the left hand side of the above expression is the moment due to horizontal component of the resultant passive thrust, P_{aH} about the pole, O. From the above equation, Y_{pp} (which is the distance of point of application of P_p from the wall top), is obtained as

$$Y_{PP} = \frac{1}{P_{pH}}\left[\left(W_{ACD} \cdot (OF + \tfrac{2}{3} \cdot DC) + W_{ADE} \cdot \overline{X}\right) + H_1 (\tfrac{2}{3} \cdot AC + FD) + P_{vP} \cdot OF - P_{pH} \cdot FD\right] \quad (38)$$

2.7.2. Pole below wall top

Referring to Fig. 3(b), by taking moments of forces and reactions about the pole, O the following equation is obtained.

$$P_{pH}(Y_{PP} - DF) = \left[\left(W_{ACD} \cdot (\tfrac{2}{3} \cdot DC - OF) - W_{ODE} \cdot \tfrac{2}{3} \cdot OF + W_{OEA}\,\overline{X}\right) + H_1 (\tfrac{2}{3} \cdot AC - DF) - P_{pV} \cdot OF\right] \quad (39)$$

In which, the terms on the right hand side of the above expression represent moment of weight of soil in the failure wedge, EACD, moment of the force H_1 and moment due to vertical component of the resultant passive thrust, P_{pV} about the pole, O. The term on the left hand side of the above expression is the moment due to horizontal component of the resultant passive thrust, P_{pH} about the pole, O. From Eq. (39), Y_{PP} (which is the distance of point of application of P_p from the wall top), is obtained as

$$Y_{PP} = \frac{1}{P_{pH}}\left[(W_{ACD} \cdot (\tfrac{2}{3} \cdot DC - OF) - W_{ODE} \cdot \tfrac{2}{3} \cdot OF + W_{OEA} \cdot \overline{X}) + H_1 (\tfrac{2}{3} \cdot AC - DF) - P_{PV} \cdot OF + P_{pH} \cdot DF\right] \quad (40)$$

The height, h of the passive thrust, P_p from the wall base is obtained as

$$h = H - Y_{PP} \quad (41)$$

3. Discussion

The basic purpose of this analysis was to compute passive pressure coefficient, K_p, location of point of application of passive thrust and study their variation with respect to the parameters involved in the analysis. It was found convenient to express the height, *h* of point of application of passive thrust from the wall base in terms of its ratio with respect to height, *H* of the retaining wall, in a non-dimensional form ($H_r = h/H$).

In Table 1, values of passive earth pressure coefficient, K_p along with angle θv (angle defining position of the pole of the log spiral on line AD) are shown for various combinations of soil friction angle, ϕ and angle of wall friction, δ. For ϕ = 20°, pole of the log spiral is located below the wall top for all the values of δ. For ϕ = 25° it goes below the wall top for higher value of δ.

3.1. Point of application of passive thrust

One distinguishing feature of the proposed method is its ability to compute the point of application of passive thrust using moment equilibrium. This has not been possible with other existing methods. In Table 2, computed values of *H*r are shown. They vary over a very narrow range, from 0.225 (for ϕ = 20° and δ = 5°) to 0.275 (for ϕ = 40° and δ = 40°).

Table 1 - Passive earth pressure coefficients and location of pole of the log spiral.

Angle of soil friction ϕ° (degrees)		Angle of wall friction δ° (degrees)							
		5	10	15	20	25	30	35	40
20	K_p	2.780	2.967	3.142	3.298				
	ϕv°	-3.880	-9.264	-14.320	-19.065				
25	K_p	3.404	3.705	4.001	4.287	4.560			
	ϕv°	6.568	1.254	-3.800	-8.622	-13.243			
30	K_p	4.196	4.655	5.126	5.606	6.090	6.572		
	ϕv°	15.405	10.167	5.132	0.276	-4.427	-9.000		
35	K_p	5.231	5.921	6.658	7.439	8.264	9.126	10.018	
	ϕv°	23.174	18.001	12.990	8.117	3.358	-1.303	-5.888	
40	K_p	6.624	7.668	8.823	10.098	11.499	13.030	14.689	16.464
	ϕv°	30.199	25.08	20.089	15.204	10.406	5.676	0.999	-3.639

Note: Negative sign of angle θ*v* refers to pole location below the wall top (Fig. 2 (b)).

Table 2 - Variation of Hr with ϕ and δ.

Angle of soil internal friction, ϕ (degrees)	Angle of wall friction, δ (degrees)							
	5	10	15	20	25	30	35	40
	Hr = h/H							
20	0.225	0.226	0.229	0.234				
25	0.235	0.235	0.237	0.241	0.248			
30	.241	0.240	0.241	0.244	0.250	0.259		
35	0.246	0.243	0.243	0.245	0.249	0.257	0.268	
40	0.249	0.245	0.243	0.244	0.247	0.253	0.262	0.275

3.2. Distribution of reactive pressure over failure surface

Another distinguishing feature of the proposed analysis is its ability to predict the distribution of reactive pressure on the failure surface using Kötter's (1903) equation. This is shown in Fig. 6 for ϕ = 40° and δ = 30°. The pressure distribution varies linearly over the straight part of the failure surface followed by curvilinear variation over the log spiral part with a maximum ordinate at the wall base.

3.3. Comparison with other solutions

In Table 3, computed values of K_p for ϕ = 20°, 30° and 40° and δ = ϕ/2 and ϕ are compared with other available solutions and in Table 4 percentage variations in the results obtained by the proposed method in comparison with other solutions are reported.

The values computed by Coulomb's (1776) theory up to ϕ = 30° and δ = ϕ/2 are lower than the proposed values in the range 2.69 to 2.92%, and up to ϕ = 30° and δ = ϕ, they are higher than the proposed values in the range 7.29 to 53.73%. For ϕ = 40° and δ = 40°, they tend to be very high with no possible comparison.

The values reported by Chen (1975) are based on limit analysis. Up to ϕ = 40° and δ = 20°, they are lower than the proposed values in the range 0 to 13.13%, and for ϕ = 40° and δ = 40°, they are higher than the proposed values by 26.97%.

Comparison with the values, which are based on rotational log spiral failure mechanism with the upper-bound theorem of limit analysis reported by Soubra & Macuh (2002) shows that, these values are lower than the proposed values in the range 2.85 to 13.5% and higher in the range 5.48 to 22.11%.

The values reported by Caquot & Kerisel (1948) are based on limit equilibrium of a log spiral mechanism. Up to ϕ = 40° and δ = 20°, they are lower than the proposed values

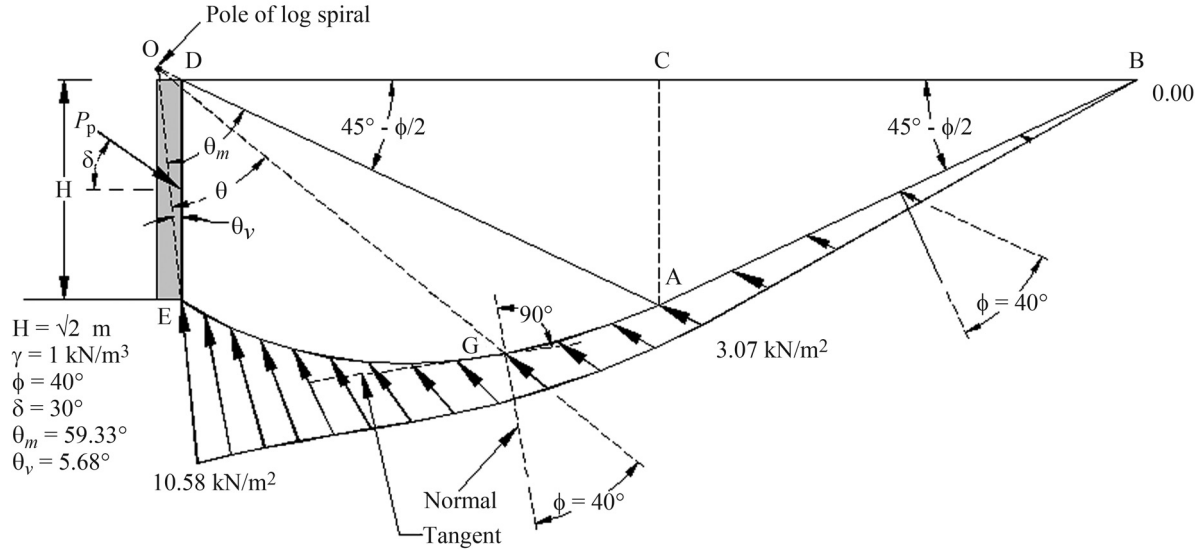

θ (degrees)	0	5	10	15	20	25	30	35	40	45	50	55	59.32
Ordinate (kN/m²)	10.58	9.16	7.96	6.93	6.07	5.35	4.75	4.26	3.87	3.56	3.33	3.16	3.07

Figure 6 - Reactive pressure distribution on the failure surface.

Table 3 - Comparison of *K*p values.

Parameters	Passive earth pressure coefficient, K_p					
Angle of soil friction, ϕ (degrees)	20		30		40	
Angle of wall friction, δ (degrees)	1/2ϕ	ϕ	1/2ϕ	ϕ	1/2ϕ	ϕ
Proposed Method	2.97	3.29	5.13	6.57	10.098	16.46
Coulomb (1776)	2.89	3.53	4.98	10.1	11.77	92.57
Caquot & Kerisel (1948)	2.60	3.01	4.50	6.42	10.36	17.5
Janbu (1957)	2.60	3.00	4.50	6.00	9.00	14.0
Sokolovski (1965)	2.55	3.04	4.62	6.55	9.69	18.2
Shield & Tolunay (1974)	2.43	2.70	4.13	5.02	7.86	11.00
Chen (1975)	2.58	3.14	4.71	7.11	10.07	20.90
Basudhar & Madhav (1980)	2.56	3.12	4.64	6.93	9.56	19.35
Kumar & Subba Rao (1997)	2.5	3.07	4.6	6.68	9.8	18.86
Soubra & Macuh (2002)	2.57	3.13	4.65	6.93	9.81	20.1
Lancellotta (2002)	2.48	2.70	4.29	5.03	8.38	11.03
Shiau *et al.* (2008) lower bound	2.50	3.02	4.38	6.58	8.79	18.64
Shiau *et al.* (2008) upper bound	2.62	3.21	4.46	7.14	10.03	20.10

in the range 2.28 to 12.45%, and for ϕ = 40° and δ = 40°, they are higher than the proposed values by 6.32%.

The values reported by Kumar & Subba Rao (1997) are based on the method of slices. Up to ϕ = 40° and δ = 20°, they are lower than the proposed values in the range 2.95 to 15.83%, and for ϕ = 40° and δ = 40°, they are higher than the proposed values by 14.58%.

The values reported by Sokolovski (1965) are based on the method of characteristics. Up to ϕ = 40° and δ = 20°, they are lower than the proposed values in the range 0.3 to 14.1% and for ϕ = 40° and δ = 40°, they are higher than the proposed values 10.57%.

Comparison with the values, which are based on limit equilibrium analysis and reported by Basudhar & Madhav (1980) shows that, these values are lower than the proposed values in the range 5.3 to 13.8% and higher in the range 5.4 to 17.5%.

With the analytical solution based on the lower bound theorem of plasticity, the K_p values as reported by Lancellotta (2002) are lower than the proposed values in the range 16.37 to 32.98%.

The K_p values reported by Shiau *et al.* (2008) using lower bound theorem coupled with finite element formulations of limit analysis and nonlinear programming techniques, are lower than the proposed values in the range 0.15 to 35.35% .The values obtained using upper bound theorem are lower than the proposed values in the range, 0.67 to 13.06% up to ϕ = 40° and δ = 20°. For ϕ and δ = 30° and ϕ and δ values of 40° and 40°, they are higher than the proposed values in the range, 8.67 to 22.11%. The possible reason for the proposed values being higher than the upper and lower bound values reported by Shiau *et al.* (2008) can be explained with the observation that, the failure surface changes from nearly a straight one to the one consisting of curved part followed by a straight line in Shiau's *et al.* (2008) method whereas, it is always a log-spiral followed by a tangent in the proposed analysis. Considering practical situations with wall friction angle in the range of one half to two third of the soil friction angle, the proposed value of K_p for δ = 1/2ϕ (ϕ = 40°) is higher by only 0.67% than the upper bound solution of Shiau *et al.* (2008). For for δ = 2/3ϕ, the proposed K_p value is higher by 6.15% than the lower bound solution and lower by 6.79% than the upper bound solution of Shiau *et al.* (2008).

Similarly, the K_p values as reported by Janbu (1957) which are based on limit equilibrium analysis are lower than the proposed values in the range 8.7 to 14.95%.

The values of K_p as reported by Shields & Tolunay (1973) are also based on limit equilibrium analysis. These values are lower than the proposed values in the range, 17.93 to 33%.

The above comparison shows that proposed values are fairly close to some of the available solutions, except those of Shields & Tolunay (1973) and Lancellotta (2002).

In Table 4, more data giving K_p values computed by Coulomb's theory (1776), Caquot & Kerisel (1948), Kumar & Subba Rao (1997), Soubra & Macuh (2002), Lancellotta (2002) and by the proposed method is reported.

It may be noted that, for the failure mechanism consisting of log spiral and its tangent, which is adopted in the proposed analysis, the K_p values are unique; since they are evaluated from the identification of a unique failure surface that satisfies force equilibrium conditions. This may be the

Table 4 - Comparison of K_p values.

Angle of friction (degrees)		Passive earth pressure coefficient *Kp*										
		Coulomb (1776)		Caquot & Kerisel (1948)		Kumar & Subba Rao (1997)		Soubra & Macuh (2002)		Lancellotta (2002)		Proposed method
Soil ϕ	Wall δ	K_p	% diff.	K_p	% diff.	K_p	% diff.	K_p	% diff.	K_p	% diff.	K_p
20		2.04	-21.5	2.04	-21.5	2.04	-21.5	2.04	-21.5	2.04	-21.5	2.60
25		2.46	-20.5	2.46	-20.6	2.46	-20.6	2.46	-20.6	2.46	-20.5	3.10
30	0	3.00	-18.9	3.03	-18.1	3	-18.9	3.00	-18.9	3.00	-18.9	3.70
35		3.69	-19.8	3.69	-19.8	3.69	-19.8	3.69	-19.8	3.69	-19.8	4.60
40		4.60	-19.3	4.59	-19.5	4.6	-19.3	4.60	-19.3	4.60	-19.3	5.70
20		2.41	-15.1	2.35	-17.4	2.38	-16.3	2.39	-16.0	2.35	-17.4	2.84
25		3.12	-13.3	3.03	-16.0	3.06	-15.1	3.07	-14.8	2.99	-17.0	3.61
30	1/3ϕ	4.14	-11.0	4.00	-14.1	4.02	-13.6	4.03	-13.4	3.89	-16.5	4.66
35		5.68	-7.8	5.28	-14.3	5.42	-12.0	5.44	-11.7	5.17	-16.1	6.16
40		8.15	-3.3	7.25	-13.9	7.58	-10.0	7.62	-9.6	7.09	-15.9	8.43
20		2.64	-11.2	2.60	-12.4	2.5	-15.7	2.57	-13.4	2.48	-16.5	2.97
25		3.55	-7.8	3.40	-11.8	3.4	-11.8	3.41	-11.5	3.22	-16.4	3.85
30	1/2ϕ	4.98	-2.9	4.50	-12.2	4.6	-10.3	4.65	-9.3	4.29	-16.3	5.13
35		7.36	4.5	6.00	-14.8	6.6	-6.3	6.59	-6.4	5.88	-16.5	7.04
40		11.8	16.6	9.00	-10.9	9.8	-3.0	9.81	-2.9	8.38	-17.0	10.10
20		2.89	-6.4	2.65	-14.1	2.73	-11.5	2.75	-10.9	2.58	-16.3	3.09
25		4.08	-0.4	3.56	-13.1	3.72	-9.2	3.76	-8.2	3.41	-16.7	4.10
30	2/3ϕ	6.11	8.9	5.00	-10.8	5.26	-6.2	5.34	-4.7	4.63	-17.4	5.61
35		9.96	24.8	7.10	-11.1	7.78	-2.5	7.95	-0.4	6.51	-18.5	7.98
40		18.7	56.0	10.7	-10.6	12.24	2.0	12.6	5.0	9.57	-20.2	12.00
20		3.53	7.1	3.01	-8.5	3.07	-6.7	3.13	-4.9	2.70	-18.0	3.29
25		5.60	22.8	4.29	-5.9	4.42	-3.1	4.54	-0.4	3.63	-20.5	4.56
30	ϕ	10.1	53.6	6.42	-2.3	6.68	1.6	6.93	5.4	5.03	-23.5	6.57
35		22.9	129	10.2	1.8	10.76	7.4	11.3	12.8	7.25	-27.6	10.02
40		92.6	462	17.5	6.3	18.86	14.6	20.1	22.1	11.03	-33.0	16.46

Percentage difference = (100 x (value obtained by other solution-value obtained by proposed method)/value obtained by proposed method).

possible reason for the variation in results obtained by the proposed method when compared to the other available solutions. The proposed method also enables the computation of point of application of passive thrust using moment equilibrium and reactive pressure distribution on the failure surface.

4. Conclusion

A method based on the application of Kötter's (1903) equation is proposed for the complete analysis of passive earth pressure on a vertical wall retaining horizontal cohesionless backfill. Kötter's (1903) equation lends itself as a powerful tool in the analysis and the results show a close agreement with some of the available solutions.

Kötter's (1903) equation facilitates identification of the unique and only possible failure surface (log-spiral followed by its tangent) using the force equilibrium conditions. The value of computed passive pressure co-efficient is therefore a unique one that can be obtained using limit equilibrium method. Another advantage of the proposed method is its ability to compute the point of application of the passive thrust using moment equilibrium which. Thus all the equations of equilibrium are effectively used in the proposed method. The distribution of soil reactions on the failure surface is also computed.

References

Balla, A. (1961) The resistance to breaking out of mushroom foundations for pylons. Proc of the 5th Int. Conf. on Soil Mechanics and Foundation Engineering, Paris, France, v. 1, pp. 569-576.

Basudhar, P.K. & Madhav, M.R. (1980) Simplified passive earth pressure analysis. Journal of the Geotechnical Engineering Division, ASCE, v. 10:GT4, p. 470-474.

Brinch Hansen, J. (1953) Earth pressure calculation. The Danish Technical Press. The Institution of Danish Civil Engineers, Copenhagen, 271 pp.

Caquot, A.I. & Kerisel, J. (1948) Tables for the Calculation of Passive Pressure, Active Pressure, and Bearing Capacity of Foundations. Libraire du Bureau des Longitudes, de L'ecole Polytechnique. Gauthier-Villars, Paris, 120 pp.

Chen, W.F. (1975) Limit Analysis and Soil Plasticity. Elsevier Science publishers, BV, Amsterdam, The Netherlands, pp. 111-146

Coulomb, C.A. (1776) Essais sur une application des regles des maximis et minimis a quelques problems de statique relatits a architecture. Mem. Acad. Roy. Pres. Divers, Sav., Paris, v. 7, p. 343-382.

Dewaikar, D.M. & Mohapatro B.G. (2003) Computation of bearing capacity factor N_γ- Terzaghi's mechanism. Int. J. Geomech., ASCE, v. 3:1, p. 123-128.

Janbu, N. (1957) Earth pressure and bearing capacity calculations by generalized procedures of slices. Proc. 4th Int. Conf. on Soil Mechanics and Foundation Engineering, London, v. 2, p. 207-212.

Kumar, J. & Subba Rao (1997) Passive pressure coefficients, critical failure surface and its kinematic admissibility. Geotechnique, v. 47:1, p. 185-192.

Kerisel, J. & Absi, E. (1990) Active and Passive Earth Pressure Tables. Balkema, Rotterdam, 220 pp.

Kötter, F. (1903) Die Bestimmung des Drucks an gekrümmten Gleitflächen, eine Aufgabe aus der Lehre vom Erddruck Sitzungsberichte der Akademie der Wissenschaften. Berlin, p. 229-233.

Lancellotta, R. (2002) Analytical solution of passive earth pressure. Géotechnique, v. 52:8, p. 617-619.

Matsuo, M. (1967) Study of uplift resistance of footings: I. Soils and Foundations, v. 7:4, p. 1-37.

Morgenstern, N.R. & Eisenstein, Z. (1970) Methods of estimating lateral loads and deformations. Proc. ASCE Speciality Conf. on Lateral Stresses in the Ground and Design of Earth-Retaining Structures, Ithaca, pp. 51-102.

Rankine, W. (1857) On the stability of loose earth. Philosophical Transactions of the Royal Society of London, v. 147, p. 9-27

Shiau, J.S.; Charles, E.A.; Andrei, V.I. and Sloan, S.W. (2008) Finite element limit analysis of passive earth resistance in cohesionless soils. Japanese Geotechnical Society, Soils and Foundations, v. 48:6, p. 843-850.

Shields, D.H. & Tolunay, A.Z. (1973) Passive pressure coefficients by method of slices. Journal of the Soil Mechanics and Foundations Division, ASCE, v. 99:SM12, Proc. Paper 10221, p. 1043-1053.

Sokolovski, V.V. (1965) Statics of Granular Media. Pergamon, Oxford, 270 pp.

Soubra, A.H. & Macuh, B. (2002) Active and passive earth pressure coefficients by a kinematical approach, Proc. of the Institution of Civil Engineers and Geotechnical Engineering., v. 155:2, p. 119-131.

Terzaghi, K. (1943) Theoretical Soil Mechanics. Wiley and Sons, New York, 510 pp.